Relativistic one-electron approach to the effect of pressure on the magnetism of $EuCo_2P_2$

Diana Guenzburger
Centro Brasileiro de Pesquisas Físicas, rua Xavier Sigaud 150, Urca, 22290-180 Rio de Janeiro, RJ, Brazil

D. E. Ellis
Department of Physics and Astronomy and Materials Research Center, Northwestern University, Evanston, Illinois 60208

J. A. Gómez
Centro Brasileiro de Pesquisas Físicas, rua Xavier Sigaud 150, Urca, 22290-180 Rio de Janeiro, RJ, Brazil
(Received 19 March 2001; published 13 November 2001)

Nonrelativistic and four-component relativistic electronic structure calculations with the discrete variational method within density functional theory were performed for embedded clusters representing the layered compound $EuCo_2P_2$, with $ThCr_2Si_2$-type structure. A relativistic one-electron model based on Kramers degeneracy was devised to describe the observed changes in the magnetism of this compound induced by applied pressure, which include the collapse of the Eu moment and the formation of Co moments. The ^{151}Eu Mössbauer isomer shift calculated with relativistic wave functions agrees well with experiment; however, the Eu^{2+}-Eu^{3+} valence change previously proposed is not predicted.

DOI: 10.1103/PhysRevB.64.214418 PACS number(s): 75.25.+z, 71.15.Rf, 76.80.+y

I. INTRODUCTION

The ternary rare-earth compounds RT_2X_2 (R=rare earth, T=Fe, Co, Ni, and X=main group element) are part of a large class of layered compounds that crystallize in the $ThCr_2Si_2$-type structure.[1,2] The layers occur in the order R-X-T-X-R.... These compounds have great interest from the point of view of magnetic properties, since they may or may not display magnetism on the T layer. When X=P, it was found that the transition-metal layer is magnetic in $PrCo_2P_2$ and $NdCo_2P_2$ (Ref. 3) and nonmagnetic in $PrFe_2P_2$ (Ref. 4) and $EuCo_2P_2$ (Ref. 5). In the latter compound, neutron diffraction measurements have shown that the Eu atoms present ferromagnetic (FM) order in the planes, with in-plane magnetic moments, and antiferromagnetic (AFM) order among the planes, with an incommensurate spiral structure along the tetragonal c axis and Néel temperature of 66.5 K. [5]

It has been demonstrated that $EuCo_2P_2$ at pressure $\cong 3.1$ GPa undergoes a structural phase transition in which there is a drastic reduction of the lattice parameter c ($\Delta c/c \cong -13\%$), accompanied by a small increase in the lattice constant a ($\Delta a/a \cong +3\%$).[6] Since this dramatic change in the structural parameters could have important consequences on the magnetic properties, high-pressure ^{151}Eu Mössbauer effect (ME) experiments were performed for this compound.[6] The Mössbauer spectrum at 4.2 K and ambient pressure shows the magnetic splitting expected for Eu^{2+} ions, in the ground state labeled $^8S_{7/2}$ in L-S coupling. At 5 GPa (above the structural phase transition), a complex spectrum is obtained derived from both magnetic and nonmagnetic Eu atoms. This spectrum was interpreted as deriving from the nonmagnetic ground state of Eu^{3+} ($^7F_0$ in L-S coupling), the magnetic component of the spectrum being due to polarization of the conduction electrons by magnetic Co atoms.[6] An ordering temperature of 260 K was obtained from the temperature dependence of the induced hyperfine field, well within the range of those obtained for the magnetic ordering of the transition-metal layers of similar compounds.[4]

In view of the intricate relations between chemical state, lattice parameters, and magnetism displayed by $EuCo_2P_2$, we have performed first-principles electronic structure calculations in the embedded cluster approach[7,8] to better understand these properties. A more complete understanding of the effect of changes in lattice parameters in $EuCo_2P_2$ will shed light on the magnetic properties of other rare-earth transition-metal compounds of similar layered structure. The relativistic four-component Dirac approach,[9] within density functional theory (DFT),[10] was chosen as appropriate for compounds with rare-earth atoms. Moreover, as described in the next section, this approach makes it possible to model the nonmagnetic Eu^{3+} ground state within a one-electron theory.

In Sec. II we briefly describe the embedded-cluster method employed, in Sec. III we present and discuss the results obtained, and in Sec. IV we summarize our conclusions.

II. THEORETICAL METHOD

The discrete variational method[7,8] (DVM) for solving the one-electron equations of DFT was employed in the embedded-cluster scheme. A 49-atom cluster was constructed according to the layered crystal structure of $EuCo_2P_2$,[1,2] centered at a Co layer represented by 13 atoms and containing above and below two Eu and two P layers represented by 6 and 12 atoms each, respectively. This Co-centered cluster was chosen primarily to investigate the magnetism of the Co layer. Local properties such as magnetic moments were obtained at the central Co, since its surroundings are best described. Figure 1 illustrates this cluster, which was embedded in the potential of approximately 700 external atoms of the solid. A different cluster with 57 atoms and an Eu layer at the center was considered to investigate the ^{151}Eu isomer shift (IS), as will be described in the next section.

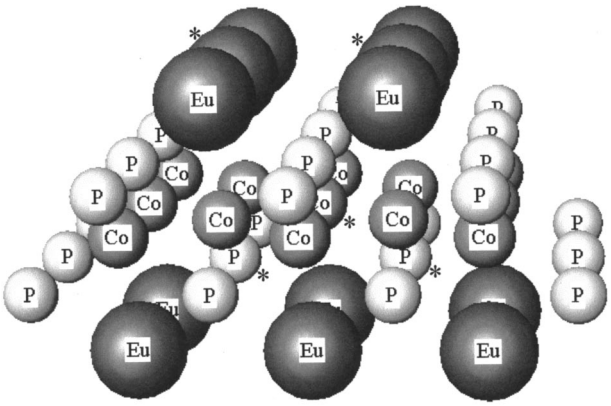

FIG. 1. Cluster $[Eu_{12}Co_{13}P_{24}]$ representing the layered compound $EuCo_2P_2$, with Co atoms at the central plane. The *c* axis is perpendicular to the Eu, Co, and P planes. Atoms marked with an asterisk are the ones included in the charge and difference density maps shown in Figs. 2 and 4, respectively.

A. Nonrelativistic scheme

In the nonrelativistic DVM,[7,8] the Kohn-Sham equations of DFT are solved self-consistently [self-consistent field (SCF)] in a three-dimensional grid of points,

$$(-\nabla^2/2+V_c+V_{\mathrm{xc}}^{\sigma})\phi_{i\sigma}(\mathbf{r})=\varepsilon_{i\sigma}\phi_{i\sigma}(\mathbf{r}), \tag{1}$$

where energies are given in Hartree atomic units. V_c is the electronic and nuclear Coulomb potential, and V_{xc}^{σ} is the spin-dependent exchange-correlation potential, for which the local functional of Vosko, Wilk, and Nusair was employed.[11] The charge density for each spin is defined as

$$\rho_{\sigma}(\mathbf{r})=\sum_i n_{i\sigma}|\phi_{i\sigma}(\mathbf{r})|^2, \tag{2}$$

where $\phi_{i\sigma}$ are the numerical spin orbitals of the cluster, with occupation number $n_{i\sigma}$ given by the Fermi-Dirac statistics. These orbitals are expanded as a linear combination of numerical symmetrized atomic orbitals (LCAO), obtained by self-consistent local density atomic calculations. The spin density $[\rho_{\uparrow}(\mathbf{r})-\rho_{\downarrow}(\mathbf{r})]$ represents the spin component of the magnetization.

In the spin-polarized or spin-unrestricted (SU) scheme, $S_z=\Sigma_i s_{zi}$ is a good quantum number; however, $\langle S^2\rangle$ is not controlled and we expect a mixture of states with $S \geqslant S_z$. This ''spin contamination'' or mixture depends upon the energy spacing of low-lying multiplets and, in the case of free molecules, is sometimes ''purified'' by spin-projection techniques. In the SU scheme neither L_z nor $\langle L^2\rangle$ are controlled, so that $|LSJ\rangle$ coupling of the Russel-Saunders type cannot be investigated. Orbital-unrestricted methods which permit control over some aspects of orbital angular momentum have been developed for atoms (m_l control) and molecules, but they are rarely applied. Furthermore, since DFT is an ensemble theory which does not normally treat individual quantum states (multiplets), procedures aimed at extraction of *L*, *S*, and *J* may be questionable on fundamental grounds.

In the DVM an error functional is defined which is minimized with respect to variations of the spin orbitals $\phi_{i\sigma}$. This leads to the usual secular equations, which were solved self-consistently in the numerical grid. In the Kohn-Sham Hamiltonian of Eq. (1), a model potential was employed, obtained by a multipolar expansion of the density centered at the cluster nuclei.[12] The multipolar expansion is determined by minimizing the least-squares error of the fit to the ''true'' density obtained by solving the Kohn-Sham equations, in each iteration, and results in a model charge density of overlapping charges centered at the nuclei. This multipolar expansion is used only in the Kohn-Sham Hamiltonian—for the final results and calculation of properties, the true density is of course considered. In the present calculations, only terms with $l=0$ were retained; it is our experience that the overlapping variationally optimized $l=0$ terms on the two sites describes rather well the final bond distribution. Our computed mean-square error in fitting the density is adequately small for the purposes of analysis of magnetic moments.

A Mulliken-type population analysis,[13] based on the coefficients of the LCAO expansion, was performed to obtain atomic orbital occupations and effective charges for the atoms in the cluster. Magnetic moments of an atom are defined as the difference in the total population for spin up and spin down. The basis was improved by performing atomic calculations to generate the basis in the configuration as obtained in the cluster by the Mulliken analysis after a preliminary set of iterations.

In the embedding procedure, the potential of the external atoms is constructed from the electron charge densities and the nuclei of the atoms surrounding the cluster. To avoid spurious migration of electrons to the exterior, the potentials of the external atoms was cut at -0.2 a.u. The Madelung potential was included with the Ewald[14] method. The charge densities of the external atoms were also optimized in the manner described for the basis.

B. Relativistic scheme

For the relativistic calculations,[9] the four-component relativistic DVM was employed,[15–17] in which the starting point is the one-electron Dirac Hamiltonian (in a.u., $c=137.037$, $m=1$, $e=1$):

$$h_D=c\alpha[\mathbf{p}-(1/c)\mathbf{A}]+c^2(\beta-1)+A_0, \tag{3}$$

where α and β are the 4×4 Dirac matrices, $\mathbf{p}=-ih\nabla$ the momentum operator, and $(\mathbf{A},A_0)$ a four-component vector potential describing external fields. We set $\mathbf{A}=0$ and $A_0=V_c+V_{xc}$, where V_c is the electron-nucleus and electron-electron Coulomb potential and V_{xc} the local exchange-correlation potential of DFT.[11] In this manner, the relativistic extension of the one-electron Kohn-Sham equations is obtained:

$$(h_D^{\mu}-\varepsilon_i^{\mu})\psi_{i\mu}(\mathbf{r},\xi)=0, \tag{4}$$

where $\psi_{i\mu}(\mathbf{r},\xi)$ is a four-component Dirac spinor and μ represents subclasses of states which we will associate with the Kramers doublets. The cluster orbitals $\psi_{i\mu}(\mathbf{r},\xi)$ are expanded on a basis of symmetrized numerical atomic orbitals (four-component central field Dirac spinors), obtained by

relativistic atomic calculations and optimized as in the nonrelativistic case. The basis was symmetrized with the use of the properties of double groups.[17] In the Dirac theory each basis function and, hence, every eigenfunction is of mixed spin ↑ and spin ↓ character—this is fundamental to relativistic quantum theory. Moreover, with the exception of *s* states, every four-component basis function contains a mixture of orbital and spin momentum, forming a well-defined total angular momentum *j*.

In relativistic theory time-reversal symmetry leads to the well-known Kramers doublets, whose degeneracy is lifted by the exchange field or by any applied magnetic field.[18] In close analogy with the spin-unrestricted scheme, one may construct a relativistic *moment-polarized* or Kramers-unrestricted (KU) scheme.[19] In a system with spherical or cylindrical symmetry, J_z is a good quantum number and the two sets of Kramers eigenfunctions have $m_j>0$ and $m_j<0$, respectively, thus clearly revealing the role of the total angular momentum $\mathbf{J}=\mathbf{L}+\mathbf{S}$ and the resulting total moments. In systems with lower symmetry, the Kramers eigenstates are obtained from properties of the corresponding double groups.

In practical terms, we introduce the densities for each component as

$$\rho_\mu=\sum_i n_{i\mu}\Psi^\dagger_{i\mu}(\mathbf{r},\xi)\Psi_{i\mu}(\mathbf{r},\xi), \tag{5}$$

with charge density $\rho_C=\rho_\uparrow+\rho_\downarrow$ and moment density $\rho_M=\rho_\uparrow-\rho_\downarrow$. We continue to use the symbols, ↑, ↓ for the Kramers components to emphasize the close analogy to the SU scheme. In fact, for $l=0$ states, the scheme reduces to spin polarization. A major advantage of the KU scheme is that spin and orbital magnetism are treated naturally and in an unbiased manner through the Dirac equation. Since time reversal is a fundamental symmetry, separation of density into ρ_μ components represents lifting of restrictions imposed on the usual Dirac SCF procedure. It is also gratifying to observe features associated with magnetic polarization, without resorting to artificial insertion of nonrelativistic Pauli spin terms into the effective Hamiltonian.[20,21] In such a procedure, sometimes denominated the ''spin-only Hamiltonian,'' the orbital magnetization may be included only by an *ad hoc* introduction of the orbital moment as additional variable; therefore, a consistent theory of orbital magnetism is missing.[21]

Here the local magnetization is defined in the usual way as

$$\mathbf{M}(\mathbf{r})=\mu_B\sum_{i\mu}\psi^\dagger_{i\mu}(g_e\mathbf{s}+\mathbf{l})\Psi_{i\mu}, \tag{6}$$

which can be displayed graphically and integrated over selected volumes to define moments. For a one-electron interpretation of magnetic moments, we resort to a simplified model, which displays the main features of localized moments. Using Mulliken atomic population analysis, we project the Dirac KU functions onto their atomic components and obtain moment populations $f^\mu_{\nu nlj}$ where (νnlj) denotes a site and the basis quantum numbers. In complete analogy with the spin-only SU scheme, we multiply the saturation moment $m_{\rm sat}=(gj)\mu_B$ by the net moment population to obtain the corresponding local moments:

$$M_{\nu nlj}=(f^\uparrow_{\nu nlj}-f^\downarrow_{\nu nlj})m_{\rm sat}$$

with the site moment

$$M_\nu=\Sigma(nlj)M_{\nu nlj}.$$

Four-component relativistic calculations within density functional theory have been recently reported by Liu and Dolg for the series of lanthanide atoms, employing the same moment polarization based on Kramers degeneracy as used here and implemented independently by them.[22] The ionization potentials obtained compare very well with experiment.

Early unrestricted Dirac-Fock (UDF) calculations for free atoms with m_j polarization by Desclaux *et al.* were highly successful in obtaining the moment polarization of the core for the determination of hyperfine interactions.[23] In the case of free atoms and systems with cylindrical symmetry, the time-reversal operator shares the same eigenfunctions with J_z; therefore the Kramers-polarized scheme corresponds to m_j polarized.

The form of the exchange-correlation potential $V^\mu_{\rm xc}\equiv V_{\rm xc}[\rho_\mu(\mathbf{r})]$, a functional of the moment density ρ_μ, employed in the relativistic calculations, was the same as in the nonrelativistic.[11] The KU exchange-correlation potentials may be viewed as an ensemble average over occupied orbitals of a given (Kramers) orientation, in exactly the same sense as in the nonrelativistic ensemble average for orbitals of a given spin orientation. The KU scheme is entirely consistent with the Dirac equation and its symmetries. Relativistic (Coulomb and Breit) corrections to the exchange potential have been derived;[20] these are expected to be quite small for valence levels of heavy elements.[21] The single-particle theory utilized here does not take into account explicitly many-particle effects. Progress has been reported in the treatment of these effects, such as the self-interaction of the electron gas,[24] relativistic atomic coupled-cluster calculations for Yb, Lu, and Lr,[25] relativistic many-body perturbation theory for atoms,[26,27] and other many-body relativistic calculations.[28] However, it is not possible to implement such rigorous treatments for solids with heavy atoms at the present time. A relativistic treatment of many-body effects in heavy atoms, taking into account the environment in the solid, is possible with the use of crystal-field theory;[29,30] however, this is not a first-principles approach.

All other features of the DVM, i.e., model potential, variational scheme, embedding, etc., are the same as in the nonrelativistic case. All SCF calculations were converged to $<10^{-3}$ in the model charge and spin (moment) densities.

III. RESULTS AND DISCUSSION

A. Electronic and magnetic properties

To investigate the effect of pressure on the magnetic properties of $EuCo_2P_2$, we performed SCF nonrelativistic calculations for the cluster depicted in Fig. 1 for the lattice parameters *a* and *c* obtained at ambient pressure ($a=3.765$ Å and

TABLE I. Charges, spin magnetic moments μ, and orbital populations of $EuCo_2P_2$ obtained with nonrelativistic spin-polarized calculations. Ionic charges are defined as the difference between the atomic number Z and the total electron population of the atom. Magnetic moments are obtained from the difference between the spin-up and spin-down populations.

		Ambient pressure		$p=\sim 3.3$ GPa	
		Population	μ (μ_B)	Population	μ (μ_B)
Co	$3d$	8.040	0.043	8.066	0.405
	$4s$	0.097	0.0	0.164	0.0
	$4p$	0.288	0.0	0.450	−0.004
Charge		+0.58		+0.32	
Eu	$4f$	6.860	6.852	6.728	6.715
	$5d$	0.154	0.035	0.177	0.032
	$6s$	0.043	0.005	0.029	0.003
	$6p$	0.034	0.003	0.034	0.003
Charge		+1.91		+2.03	
P	$3s$	1.906	0.0	1.843	0.0
	$3p$	4.473	0.0	4.312	−0.020
Charge		−1.38		−1.16	

$c=11.348$ Å) and at pressure of ~3.3 GPa ($a\cong 3.84$ Å and $c\cong 9.59$ Å).[6,31] AFM coupling was induced among the Eu layers (and FM coupling within each layer), in order to model the neutron scattering results.[5] In L-S coupling the ground state of Eu^{2+} ($4f^7$) is ${}^8S_{7/2}$; i.e., magnetic with $J=7/2$, while the excited Eu^{3+} ($4f^6$) state is nonmagnetic, ${}^7F_0$. As we have discussed above, in the nonrelativistic one-electron picture there is no way of representing the coupling of L and S to produce a specific J. In the SU scheme, the strong $4f$ localization and resulting strong exchange forces tend to align all $4f$ electrons to produce a high-spin magnetic configuration in all cases. Therefore SU calculations correctly predict high spin for both Eu^{2+} and Eu^{3+}, but are unable to describe the counterbalancing ($J=|L-S|$) orbital contributions.

For the nonrelativistic calculations, the basis set employed contained the orbitals $3d$, $4s$, and $4p$ on Co, $4f$, $5d$, $6s$, and $6p$ on Eu, and $3s$ and $3p$ on P. Convergence of the $4f$ was achieved by employing a significant ''thermal broadening'' in the SCF iterations over the narrow band of $4f$ levels at the Fermi level. The ''thermal broadening'' was gradually decreased until almost totally removed in successive sets of iterations, to the point that decreasing it further did not change the results. Core orbitals were kept ''frozen'' after the first iteration, and valence orbitals were explicitly orthogonalized to the core.

In Table I are given the charges and orbital populations obtained with the nonrelativistic calculations for lattice parameters at ambient pressure and ~3.3 GPa. In both cases a large spin on Eu is obtained. The populations on Eu show a significant hybridization of the $4f$ with $5d$, less with $6s$ and $6p$. The $4f$-$5d$ hybridization becomes slightly higher with applied pressure, as would be expected. Pressure causes a significant decrease of the positive charge on Co by filling the $4s$ and $4p$ orbitals. The charge on Eu, however, increases only by +0.12, far less than the $1e$ proposed in the qualitative Eu^{3+} model. The P ions became somewhat less negative.

TABLE II. Charges and orbital populations of $EuCo_2P_2$ obtained with relativistic calculations. Ionic charges are defined as the difference between the atomic number Z and the total electron populations of the atom.

		Ambient pressure Population		$p=\sim 3.3$ GPa Population	
Co	$3d_{3/2}$	3.262	8.029	3.270	8.069
	$3d_{5/2}$	4.767		4.799	
	$4s_{1/2}$	0.114		0.177	
	$4p_{1/2}$	0.115	0.334	0.181	0.518
	$4p_{3/2}$	0.219		0.337	
Charge		+0.52		+0.24	
Eu	$4f_{5/2}$	5.878	6.531	5.867	6.386
	$4f_{7/2}$	0.653		0.519	
	$5d_{3/2}$	0.116	0.274	0.120	0.286
	$5d_{5/2}$	0.158		0.166	
	$6s_{1/2}$	0.103		0.068	
	$6p_{1/2}$	0.022	0.054	0.018	0.045
	$6p_{3/2}$	0.032		0.027	
Charge		+2.04		+2.22	
P	$3s_{1/2}$	1.900		1.833	
	$3p_{1/2}$	1.527	4.560	1.471	4.391
	$3p_{3/2}$	3.033		2.920	
Charge		−1.46		−1.22	

To start the iterations, a spin magnetic moment of $0.6\mu_B$ was induced on the Co atoms in both cases; this moment practically disappeared in the self-consistent procedure for the calculation at ambient pressure. For the calculation at higher pressure, however, moments on the Co atoms were maintained. For the central Co atom, whose environment is best described in the cluster, the value is $0.4\mu_B$; other atoms in the plane are also magnetic, but in some cases with negative moments. Although atoms on the surface of the cluster suffer from spurious bond-truncation effects, this AFM coupling obtained in the SCF procedure suggests a complex magnetic structure within the Co layers.

This result shows that the changes in the lattice parameters brought on by applied pressure favor the appearance of magnetism in the Co layers, as indicated by experiment.[6] That this effect may already be seen at the nonrelativistic level indicates that relativistic effects play no major role in the pressure-induced magnetization of Co.

Table II shows the orbital occupations and charges for the relativistic calculations in which no polarization is considered. For these calculations, both $4f_{5/2}$ and $4f_{7/2}$ were included in the variational space. The other orbitals of the basis are Eu $5d_{3/2}$, $5d_{5/2}$, $6s_{1/2}$, $6p_{1/2}$, and $6p_{3/2}$; Co $3d_{3/2}$, $3d_{5/2}$, $4s_{1/2}$, $4p_{1/2}$, and $4p_{3/2}$; and P $3s_{1/2}$, $3p_{1/2}$, and $3p_{3/2}$. Results are given for the innermost atoms, as explained previously. Due to the spin-orbit interaction, the $f_{5/2}$ has lower energy than $f_{7/2}$ in the atom and solid; accordingly, its population in the solid reaches almost the maximum value

TABLE III. Charges, orbital populations, and moments of $EuCo_2P_2$ obtained with moment-polarized relativistic calculations. Ionic charges are defined as the difference between the atomic number Z and the total electron population of the atom. Orbital moments are defined as the difference in the populations of each component of the Kramers doublet, times gj of the corresponding orbital. Eu $4f_{5/2}$ is ''frozen'' in the core with six electrons.

		Ambient pressure		$p=\sim 3.3$ GPa	
		Population	μ (μ_B)	Population	μ (μ_B)
Co	$3d_{3/2}$	3.265	0.080	3.232	0.280
	$3d_{5/2}$	4.749 } 8.014	0.315 } 0.395	4.756 } 7.988	1.104 } 1.384
	$4s_{1/2}$	0.100	0.001	0.186	0.003
	$4p_{1/2}$	0.113	0.0	0.235	0.0
	$4p_{3/2}$	0.215 } 0.328	−0.002 } −0.002	0.472 } 0.707	−0.006 } −0.006
	Charge: +0.56		$\mu_T=0.39$	Charge: +0.12	$\mu_T=1.38$
Eu	$4f_{5/2}$	6.0	⋯	6.0	⋯
	$4f_{7/2}$	0.550 } 6.550	1.700 } 1.700	0.396 } 6.396	0.132 } 0.132
	$5d_{3/2}$	0.125	0.007	0.129	0.0
	$5d_{5/2}$	0.172 } 0.297	0.027 } 0.034	0.178 } 0.307	0.0 } 0.0
	$6s_{1/2}$	0.116	0.008	0.043	0.001
	$6p_{1/2}$	0.018	0.0	0.019	0.0
	$6p_{3/2}$	0.027 } 0.045	0.002 } 0.002	0.031 } 0.050	0.0 } 0.0
	Charge: +1.99		$\mu_T=1.74$	Charge: +2.20	$\mu_T=0.13$
P	$3s_{1/2}$	1.894	0.001	1.784	0.0
	$3p_{1/2}$	1.526	0.001	1.461	0.0
	$3p_{3/2}$	3.043 } 4.569	0.008 } 0.009	2.901 } 4.362	0.030 } 0.030
	Charge: −1.46		$\mu_T=0.01$	Charge: −1.15	$\mu_T=0.03$

6, both for ambient and applied pressure. Only a fraction of one electron occupies the $4f_{7/2}$ orbital. Comparison with Table I shows little difference in the populations and charges for Co and P; for Eu, a slight increase in the $4f$-$(5d,6s,6p)$ hybridization occurs in the relativistic case, resulting in a smaller total $4f$ population for both pressures. This is due to the known relativistic effect of expansion of the $4f$ orbital and concomitant s,p contraction. Positive charges on Eu are somewhat higher in the relativistic case.

To investigate the magnetic properties with the relativistic KU theory, we removed the restriction of Kramers degeneracy as described above.[8,14–18] The driving force of the polarization is the same exchange-correlation potential as in the nonrelativistic case.[11] We shall simply call these calculations and the derived wave functions ''moment polarized''; alternatively, a perhaps more rigorous denomination would be ''Kramers polarized.''

To model the magnetic and nonmagnetic states of the Eu ions, we focused on the value of J of the states $^8S_{7/2}$ (Eu^{2+}) and $^7F_0$ (Eu^{3+}) and its relationship to properties of the one-electron density functional distribution. A state with $J=7/2$ may be constructed with the one-electron configuration $(f_{5/2})^p(f_{7/2})^q$ with seven electrons by completely filling the $4f_{5/2}$ orbital and placing the remaining electron in the $4f_{7/2}$. The removal of the latter (or quenching of its polarization) will result in $J=0$. However plausible from the point of view of energetics, this scheme would lead also to the conclusion that $L=3$, $S=1/2$ for f^7 and $L=0$, $S=0$ for f^6, contrary to the actual many-electron state quantum numbers. As mentioned previously, the nonrelativistic SU scheme correctly gives $S=7/2$ and $S=3$ in these cases, but gives no information on L. A rigorous analysis of the local magnetism at Eu sites would require the construction of proper many-electron wave functions using the local double-group symmetry. However, this would take us beyond the domain of DFT.

As the nonpolarized calculation has shown (Table II), the spin-orbit splitting of the $4f$ levels is enough to result in the almost complete filling of the lower energy $4f_{5/2}$. Therefore, initially we performed SCF moment-polarized calculations keeping the Eu $4f_{5/2}$ of the basis in the valence space, as in the nonrelativistic calculations. However, it soon became clear that the failure of the ''standard'' exchange-correlation potential to deal adequately with the strong (l-l) electron correlation within the $4f$ orbital resulted in an exchange splitting much larger than the spin-orbit. Consequently, for these calculations the electrons filled preferentially the orbitals pertaining to the same members of the Kramers doublet, resulting in much higher values of J. To obtain the configurations that may lead to the desired values of J, we therefore kept the $4f_{5/2}$ orbital completely filled and ''frozen'' in the core in the polarized calculations.

In Table III are given the charges, populations, and magnetic moments obtained in the polarized relativistic calculations. The g factor of a given atomic orbital is given by the well-known expression (with $s=1/2$)

$$g=1+\frac{j(j+1)+s(s+1)-l(l+1)}{2j(j+1)}. \tag{7}$$

Comparing the electron populations and charges given in

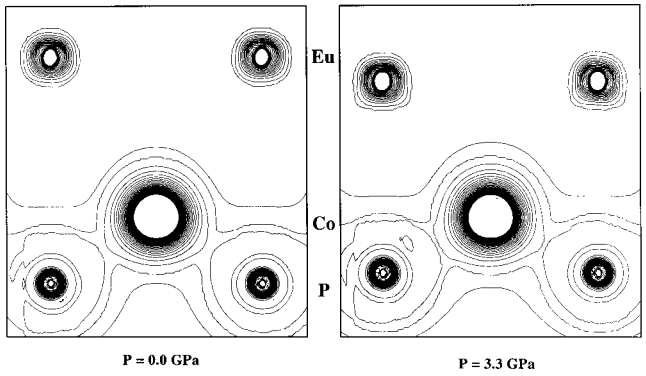

FIG. 2. Electronic charge density maps obtained from the relativistic polarized calculations, on a plane containing the *c* axis, perpendicular to the Eu, Co, and P planes. This plane intersects nuclei of Eu, Co, and P atoms, marked with an asterisk in Fig. 1. Contours are from 0 to 1, with intervals $0.0333e/a_0^3$.

Table III with Table II, we see that the main change brought in by the polarization is an even smaller positive charge on Co induced by pressure (and thus a more metallic character of the bonding in the Co plane), due mainly to a larger $4p$ population. Other than this, charges and populations are very similar in the two sets of calculations. The decrease of the positive charge on Co is accompanied by a decrease of the magnitude of the negative charge on P. Thus the bond between Co and P becomes more covalent in nature. In Fig. 2 are shown electron charge density maps on a plane along the *c* axis. It may be observed that the Eu ions are quite isolated; lines show the quite strong covalent bonding between Co and P. One striking result is that, for all three sets of calculations (nonrelativistic, relativistic, and relativistic polarized), the increase of the positive charge on Eu brought in by pressure is quite small (maximum +0.2), all charges obtained being close to +2.

In the polarized calculations, a net 0.6 polarized electrons were placed initially in the $3d$ orbitals of the Co atoms (corresponding to $1.35\mu_B$) and one polarized electron in the Eu $4f_{7/2}$ (corresponding to $4.0\mu_B$). After the SCF iterations, for the calculations at ambient pressure the moments on the Co atoms were reduced considerably; on Eu, the initial moment was reduced to slightly less than half, due mainly to depletion of the $4f_{7/2}$ orbital resulting from the hybridization with the valence orbitals. For the calculations with applied pressure, on the contrary, the initial moment on Co is slightly increased after the SCF iterations, whereas the moment on Eu almost disappears. Therefore, it is seen that this one-electron relativistic theory is capable of reproducing the experimentally observed magnetic behavior of $EuCo_2P_2$ with and without applied pressure.[6] It should be observed, however, that the maximum possible value of μ for Eu in this model is $4\mu_B$, and not $7\mu_B$ as in the *L-S* coupling state ${}^8S_{7/2}$.

The changes in the magnetism of $EuCo_2P_2$ induced by pressure may be visualized better by density of states (DOS) diagrams and electron density maps. DOS in the DV cluster method are obtained by enlarging the discrete energy levels of the cluster with Lorentzians.[8] In Fig. 3 are depicted the

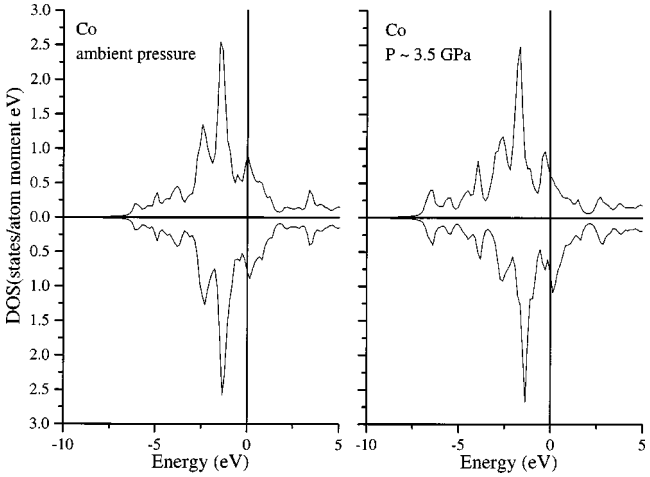

FIG. 3. Valence $(3d+4s+4p)$ DOS of Co (central atom in the plane) obtained with the relativistic polarized calculations. The upper part of figure shows the DOS of positive moment levels; the lower part shows the DOS of negative moment levels.

DOS at Co with and without applied pressure. It may be seen that a secondary peak is present at the Fermi energy, and this is polarized in the solid under pressure. Similar peaks in the region of the Fermi energy were found for the Ni DOS in calculations for the layered compounds RNi_2B_2C,[32,33] some of which present superconductivity. In Fig. 4 is displayed a map of the density of the relativistic polarized electrons on a plane containing the *c* axis. The effect of pressure on the magnetism is quite clear, suppressing the moments on Eu and enhancing those on Co. The same effect may be seen on relativistic polarized electrons density maps on the Eu plane (Fig. 5) and on the Co plane (Fig. 6).

B. Isomer shifts

^{151}Eu ME experiments revealed a large change in the IS with applied pressure, which was interpreted as deriving from a change on the charge on the Eu ions from +2 to +3.[6] Since our electronic structure calculations did not show such

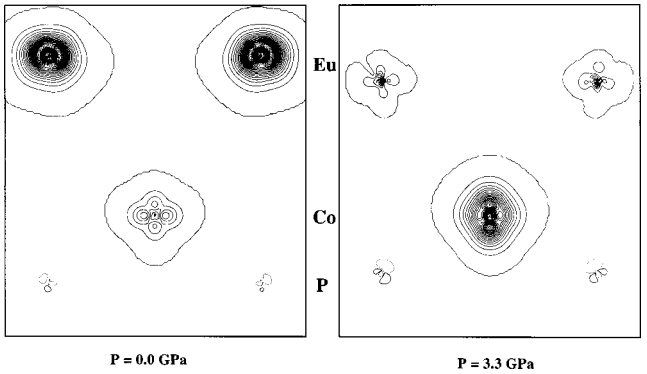

FIG. 4. Kramers-polarized electrons difference density maps obtained from the relativistic polarized calculations, on a plane containing the *c* axis, perpendicular to the Eu, Co, and P planes. This plane intersects nuclei of Eu, Co, and P atoms, marked with an asterisk in Fig. 1. Contours are from 0.001 to 0.25 and from −0.001 to −0.25, with intervals $0.0083e/a_0^3$.

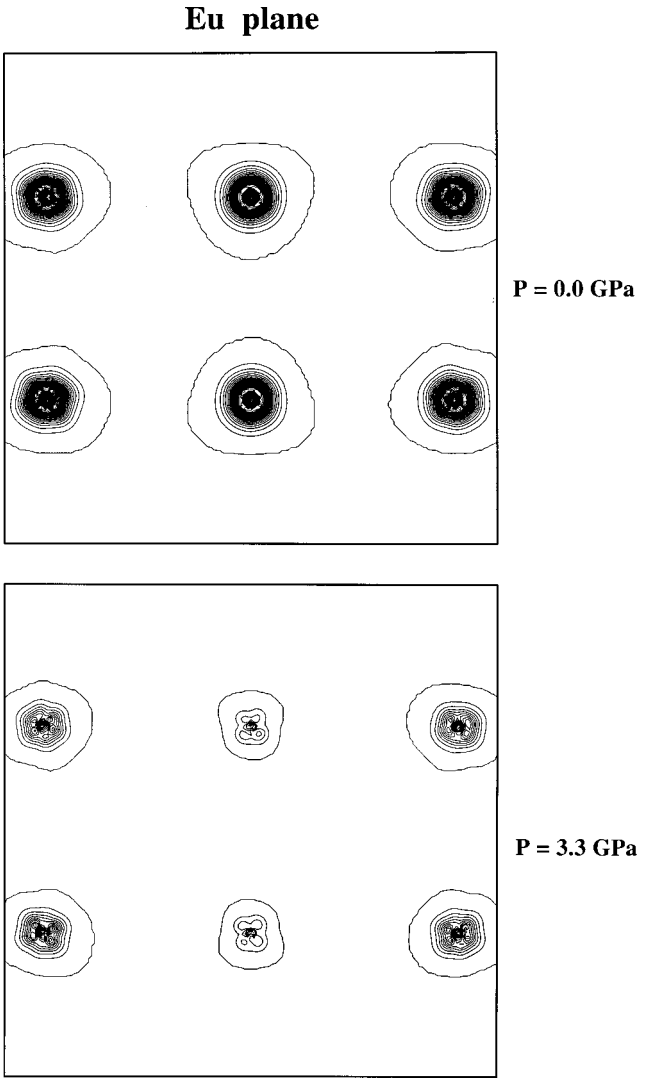

FIG. 5. Kramers-polarized electrons difference density maps obtained from the relativistic polarized calculations, on one of the Eu planes. Contour specifications as in Fig. 4.

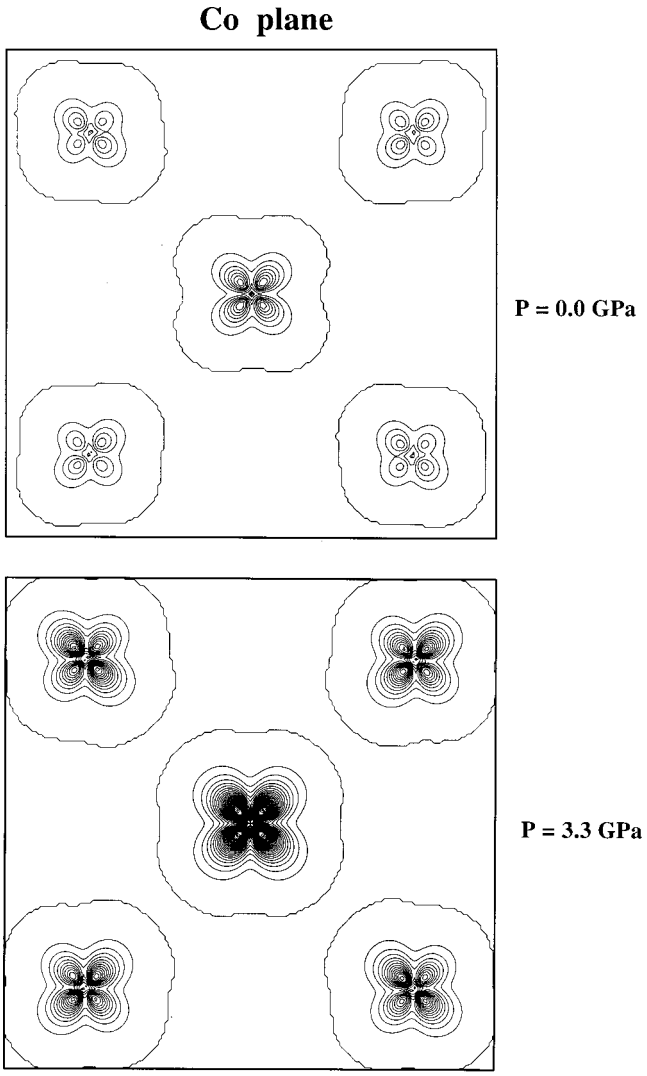

FIG. 6. Kramers-polarized electrons difference density maps obtained from the relativistic polarized calculations, on the Co plane. Contours are from 0.001 to 0.5 and from -0.001 to -0.5, with intervals $0.0166e/a_0^3$.

a large change in the charge, we have calculated the IS using the relativistic SCF charge densities. The IS is defined as[34]

$$\mathrm{IS}=\tfrac{2}{3}\pi Ze^2\Delta\langle r_N^2\rangle\Delta\rho(0)\equiv\alpha\Delta\rho(0). \tag{8}$$

No significant changes in this expression are needed in a relativistic theory.[35]

To calculate the IS, another embedded cluster, with 57 atoms, was considered, especially designed for this purpose; this is depicted in Fig. 7. In this cluster, a layer of Eu is placed at the center; the IS is calculated at the central Eu atom, whose environment is most similar to that in the bulk solid. Both nonpolarized and polarized relativistic calculations were performed, with the same atomic orbitals in the valence basis set as for the other cluster, to which were added the Eu $5s_{1/2}$ and $5p_{1/2}$, which are essential for calcu-

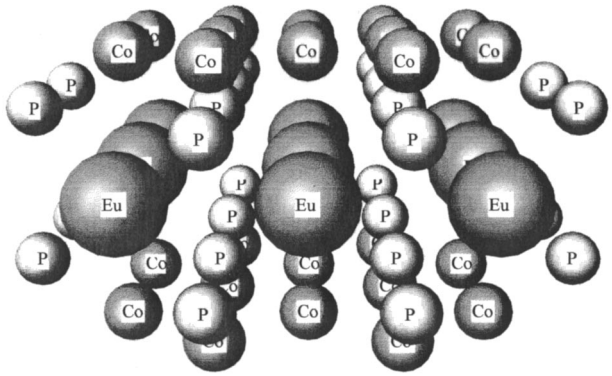

FIG. 7. Cluster $[Eu_9Co_{24}P_{24}]$ representing the layered compound $EuCo_2P_2$, with Eu atoms at the central plane. The c axis is perpendicular to the Eu, Co, and P planes.

TABLE IV. Theoretical and experimental isomer shifts.

	$EuCo_2P_2$		
	Nonpolarized relativistic		
Applied pressure (GPa)		$\rho(0)(a_0^{-3})$	$\Delta\rho(0)(a_0^{-3})$
~3.3	$1s_{1/2}$-$4p_{1/2}$	578 431.07	
	Valence	624.06	
	Total	579 055.13	26.06
0.0	$1s_{1/2}$-$4p_{1/2}$	578 430.86	
	Valence	598.21	
	Total	579 029.07	
	Polarized relativistic		
Applied pressure (GPa)		$\rho(0)(a_0^{-3})$	$\Delta\rho(0)(a_0^{-3})$
~3.3	$1s_{1/2}$-$4p_{1/2}$	578 431.05	
	Valence	611.34	
	Total	579 042.39	18.15
0.0	$1s_{1/2}$-$4p_{1/2}$	578 430.86	
	Valence	593.38	
	Total	579 024.24	
Eu^{3+}		579 026.34	34.21
Eu^{2+}		578 992.13	
$\Delta IS(EuF_3-EuF_2)=+13.58$ mm/s[a] $\therefore \alpha=0.397$ mm a_0^3/s			
$EuCo_2P_2$-ΔIS (mm/s)			
Nonpolarized relativistic	+10.34		
Polarized relativistic	+7.20		
Experimental	+7.71 ($T=300$ K)[b]		
	+9.80 ($T=4.2$ K)[b]		

[a]From Reference 36.

[b]From Reference 6.

lating the IS.[36] $\Delta\rho(0)$ is a small difference between two very large numbers; therefore, after optimization the basis obtained for ambient pressure was used in all cases to assure the cancellation of numerical errors necessary in the calculation of $\Delta\rho(0)$. In addition, a more precise polynomial grid of points is constructed inside a sphere of radius 2.0 a.u. centered at the nucleus of the central Eu to assure a better description of the wave functions in the core region. In the relativistic theory, all orbitals $s_{1/2}$ and $p_{1/2}$ penetrate the nucleus. To obtain the contribution from the core orbitals $1s_{1/2}$-$4p_{1/2}$, which are ''frozen'' in the cluster calculations, atomic SCF calculations were performed for Eu ions with the SCF orbital populations obtained for the cluster. A finite radius $R=1.2A^{1/3}$ fm$=6.3903$ fm was considered for the nucleus of ^{151}Eu, which is necessary to obtain finite values of the wave functions at the origin. To obtain the parameter α in Eq. (8), free-ion SCF calculations were performed for Eu^{2+} and Eu^{3+} and related to the experimental IS values of EuF_2 and EuF_3, respectively.[36] These compounds were chosen since they may be considered to contain the most ionic bonds, and thus the free-ion approximation is more justifiable. Furthermore, deriving α with values of $\rho(0)$ obtained with the same methodology assures considerable cancellation of errors.

The results are summarized in Table IV. For this cluster, the change of the Eu ionic charge induced by pressure was even smaller than for the previous cluster (from +1.91 to +1.99). It is seen that the theoretical numbers obtained for the IS are in the range of the experimental values. Since our electronic structure calculations do not take the temperature into account, it is more coherent to compare with the experimental value at 4.2 K. As for the two theoretical values (nonpolarized and polarized), in principle the polarized calculation is a better approximation, due to the added degree of freedom. On the other hand, as explained earlier, only in the nonpolarized calculation are both the $4f_{5/2}$ and $4f_{7/2}$ kept in the valence space. Since the $4f$ orbitals play a significant role in the isomer shift, due to their shielding of the $s_{1/2}$ and $p_{1/2}$ electrons,[36] the nonpolarized model may be thought of as more complete for the determination of the IS. In this case, the accord between theory and experiment is seen to be excellent.

We have therefore seen that the theory is capable of reproducing the experimentally found change in the ^{151}Eu IS of $EuCo_2P_2$ induced by pressure. On the other hand, we have also shown that this change in the IS is not due to a change from ionic charge +2 to +3, since the theoretical charges obtained are all around +2. Therefore, the increase of $\Delta\rho(0)$ with pressure must be due to a pressure-induced compression of the wave functions, brought on by the pronounced decrease of the interatomic distances along the c axis, analogous to volume effects[37] observed in metals. This compression of the wave functions at shorter interatomic distances ($\equiv$ higher pressure) is a consequence of the Pauli exclusion

principle, which causes a distortion towards a higher amplitude near the Eu nuclei, due to increased orthogonality effects with the neighbor atoms. This well-known volume effect is sometimes denominated ''overlap distortion.'' [38]

IV. CONCLUSIONS

We have performed nonrelativistic and four-component relativistic electronic structure calculations with the discrete variational method in density functional theory for embedded clusters representing the layered compound $EuCo_2P_2$. The relativistic one-electron model devised has proved to be adequate for describing the magnetic behavior of this compound with applied pressure. The calculations showed that the effect of applied pressure on $EuCo_2P_2$ is to suppress the magnetic moments on Eu and, inversely, develop magnetism on the Co layer. The ionic charge on Eu, however, does not change significantly with pressure, remaining approximately $+2$. The change on the ^{151}Eu Mössbauer isomer shift induced by pressure does not correspond to a change in the oxidation state of Eu from $+2$ to $+3$, but rather is promoted by distortion of the wave functions caused by decreased interatomic distances along the *c* axis.

ACKNOWLEDGMENTS

This work was supported in part by CNPq and by the National Science Foundation through the Materials Research Center at Northwestern University, Grant No. DMR-0076097.

[1] R. Marchand and W. Jeitschko, J. Solid State Chem. **24**, 351 (1978).
[2] E. Parthé and B. Chabot, in *Handbook of the Physics and Chemistry of Rare Earths*, edited by K. A. Gschneidner, Jr. and L. Eyring (Elsevier, Amsterdam, 1984).
[3] E. Mörsen, B. D. Mosel, W. Müller-Warmuth, M. Reehuis, and W. Jeitschko, J. Phys. Chem. Solids **49**, 785 (1988).
[4] M. Reehuis and W. Jeitschko, J. Phys. Chem. Solids **51**, 961 (1990).
[5] M. Reehuis, W. Jeitschko, M. H. Möller, and P. J. Brown, J. Phys. Chem. Solids **53**, 687 (1992).
[6] M. Chefki, M. M. Abd-Elmeguid, H. Micklitz, C. Huhnt, W. Schlabitz, M. Reehuis, and W. Jeitschko, Phys. Rev. Lett. **80**, 802 (1998).
[7] D. E. Ellis, Int. J. Quantum Chem. **2S**, 35 (1968); D. E. Ellis and G. S. Painter, Phys. Rev. B **2**, 2887 (1970).
[8] D. E. Ellis and D. Guenzburger, Adv. Quantum Chem. **34**, 51 (1999), and references therein.
[9] M. E. Rose, *Relativistic Electron theory* (Wiley, New York, 1961); P. Strange, *Relativistic Quantum Mechanics* (Cambridge University Press, Cambridge, England, 1998).
[10] R. G. Parr and W. Yang, *Density Functional Theory of Atoms and Molecules* (Oxford University Press, New York, 1989).
[11] S. H. Vosko, L. Wilk, and M. Nusair, Can. J. Phys. **58**, 1200 (1980).
[12] B. Delley and D. E. Ellis, J. Chem. Phys. **76**, 1949 (1982).
[13] R. S. Mulliken, J. Chem. Phys. **23**, 1833 (1955); **23**, 1841 (1955).
[14] C. Kittel, *Introduction to Solid State Physics*, 7th ed. (Wiley, New York, 1996), Appendix B.
[15] D. E. Ellis, J. Phys. B **10**, 1 (1977).
[16] A. Rosén and D. E. Ellis, J. Chem. Phys. **62**, 3039 (1975).
[17] D. E. Ellis and G. L. Goodman, Int. J. Quantum Chem. **25**, 185 (1984).
[18] E. P. Wigner, *Group Theory* (Academic, New York, 1960).
[19] A. Rosén, D. E. Ellis, H. Adachi, and F. W. Averill, J. Chem. Phys. **65**, 3629 (1976).
[20] A. H. MacDonald and S. H. Vosko, J. Phys. C **12**, 2977 (1979).
[21] M. Richter, in *Handbook of Magnetic Materials*, edited by K. H. J. Buschow (Elsevier, Amsterdam, in press).
[22] W. Liu and M. Dolg, Phys. Rev. A **57**, 1721 (1998).
[23] J. P. Desclaux, A. J. Freeman, and J. V. Mallow, J. Magn. Magn. Mater. **5**, 265 (1977).
[24] B. Holm and U. von Barth, Phys. Rev. B **57**, 2108 (1998).
[25] E. Eliav, U. Kaldor, and Y. Ishikawa, Phys. Rev. A **52**, 291 (1995).
[26] W. R. Johnson, S. A. Blundell, and J. Sapirstein, Phys. Rev. A **37**, 2764 (1988).
[27] Y. Ishikawa and K. Koc, Phys. Rev. A **53**, 3966 (1996).
[28] I. Lindgren, Phys. Scr. **T34**, 36 (1991).
[29] L. Smentek, B. G. Wybourne, and J. Kobus, J. Phys. B **34**, 1513 (2001).
[30] J. A. Tuszynskija and J. M. Dixon, Physica A **156**, 924 (1989).
[31] H. Micklitz (private communication).
[32] Z. Zeng, D. E. Ellis, D. Guenzburger, and E. Baggio-Saitovitch, Phys. Rev. B **54**, 13 020 (1996).
[33] Z. Zeng, D. E. Ellis, D. Guenzburger, and E. M. Baggio-Saitovitch, Phys. Rev. B **53**, 6613 (1996).
[34] N. N. Greenwood and T. C. Gibb, *Mössbauer Spectroscopy* (Chapman and Hall, London, 1971).
[35] B. D. Dunlap and G. M. Kalvius, in *Mössbauer Isomer Shifts*, edited by G. K. Shenoy and F. E. Wagner (North-Holland, Amsterdam, 1978).
[36] E. R. Bauminger, G. M. Kalvius, and I. Nowik, in *Mössbauer Isomer Shifts*, edited by G. K. Shenoy and F. E. Wagner (North-Holland, Amsterdam, 1978).
[37] D. Guenzburger and D. E. Ellis, Phys. Rev. B **31**, 93 (1985).
[38] *Mössbauer Isomer Shifts*, edited by G. K. Shenoy and F. E. Wagner (North-Holland, Amsterdam, 1978).